THE JOURNAL OF PHYSICAL CHEMISTRY C

Article

Cite This: J. Phys. Chem. C 2020, 124, 1171−1177

pubs.acs.org/JPCC

Free Triplets Versus Bound Triplet−Triplet Biexciton in Intramolecular Singlet Fission Materials: Structure−Property Correlations

Souratosh Khan[†] and Sumit Mazumdar*[,‡,§,∥]

[†]School of Information, [‡]Department of Physics, [§]Department of Chemistry and Biochemistry, and [∥]College of Optical Sciences, University of Arizona, Tucson, Arizona 85721, United States

Supporting Information

ABSTRACT: Recent advances in singlet-fission research make it imperative that structure−property correlations that determine the optical signatures of the triplet−triplet spin biexciton as well as its binding energy be understood precisely. We report many-body calculations of excited-state absorptions from the triplet exciton and the triplet−triplet biexciton from two transversally linked dimers of pentacene derivatives. Comparison of experiment against theory leads to new interpretations of experiments performed earlier. We show that in the para-linked isomer, the triplet−triplet does not dissociate to free triplets through the duration of the measurements. In contrast, even as calculated and experimental transient absorptions agree in the meta isomer, the experimental observations here are more difficult to interpret, indicating the strong role structural variations play in determining the rate and yield of free triplets. We also report many-body calculations of the spin gap, defined as the energy difference between the spin-quintet versus spin-singlet triplet−triplet, as well as the binding energy of the spin-singlet triplet−triplet, defined as the energy difference between two free triplets and the bound biexciton. The spin gap and the binding energy of the spin-singlet triplet−triplet are different quantities in all but coupled two-level systems. The experimental behavior in the transversally linked dimers as well as previously studied longitudinally linked dimers agrees with the trends that would be predicted from the computed biexciton binding energies.

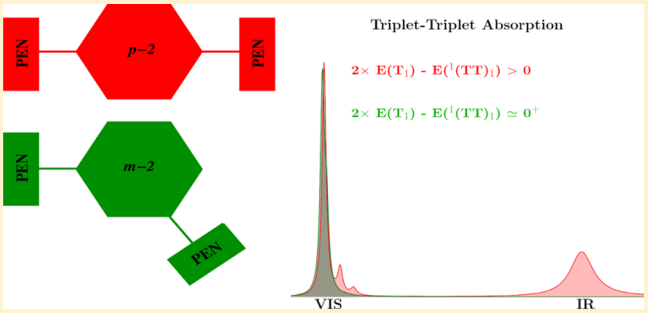

INTRODUCTION

Singlet fission (SF) is a photophysical process that involves the generation of two spin-triplet excitons (T_1) from a single optically accessible singlet exciton (S_1) in an organic π-conjugated molecule. As the process generates four charge carriers per absorbed photon, it is being intensively investigated[1−4] as a possible means to overcome the Shockley−Queisser limit[5] for the efficiencies of single-junction organic solar cells. SF requires excitations across multiple chromophore molecules, and interest has shifted in recent years from intermolecular to intramolecular SF (ISF) in covalently linked chromophore molecules.[6−17] Very recently, experimental research has been extended to oligomers consisting of up to five acene monomers, which are not all same.[18]

SF is a spin-allowed multistep process in which the S_0S_1 state (here S_0 is the monomer ground state) first relaxes to a bound triplet−triplet biexciton $^1(TT)_1$ that is overall spin-singlet (here the superscript and subscript refer to the spin multiplicity and the quantum number of the state within the triplet−triplet space, respectively). We note that $^1(TT)_1$ is in the even spatial parity spin-singlet subspace and can occur below S_1. Our nomenclature allows a clear distinction between one- and two-photon spin-singlet states. $^1(TT)_1$, nominally a double excitation within the molecular orbital (MO) theory,[19] is often degenerate with or even lower in energy than S_0S_1 because of strong Hubbard repulsion among π-electrons occupying the same p_z orbital.[20−22] SF should be considered complete only when $^1(TT)_1$ further dissociates into a pair of free triplets T_1. In ISF, the assumption has often been that $^1(TT)_1$ is weakly bound, and triplet energy transfer will occur from the photoexcited dimer to a neighboring dimer in its ground state, leading to two free triplets.

Because $^1(TT)_1$ and T_1 are both optically inaccessible from the ground state, they are identified from ultrafast excited-state spectroscopy. One key question in SF is then whether or not there exist experimental optical signatures of the bound $^1(TT)_1$ biexciton that are distinct from those of T_1. Identification of unique optical signatures of $^1(TT)_1$ is essential for the determination of its lifetime. Further, the dissociation efficiency of $^1(TT)_1$ depends on its binding energy E_b, defined as the energy difference between the two free triplets and the triplet−triplet,[23,24] $2 \times E(T_1) - E(^1(TT)_1)$. Structural features

Received: October 21, 2019
Revised: December 6, 2019
Published: December 11, 2019

DOI: 10.1021/acs.jpcc.9b09831
J. Phys. Chem. C 2020, 124, 1171−1177

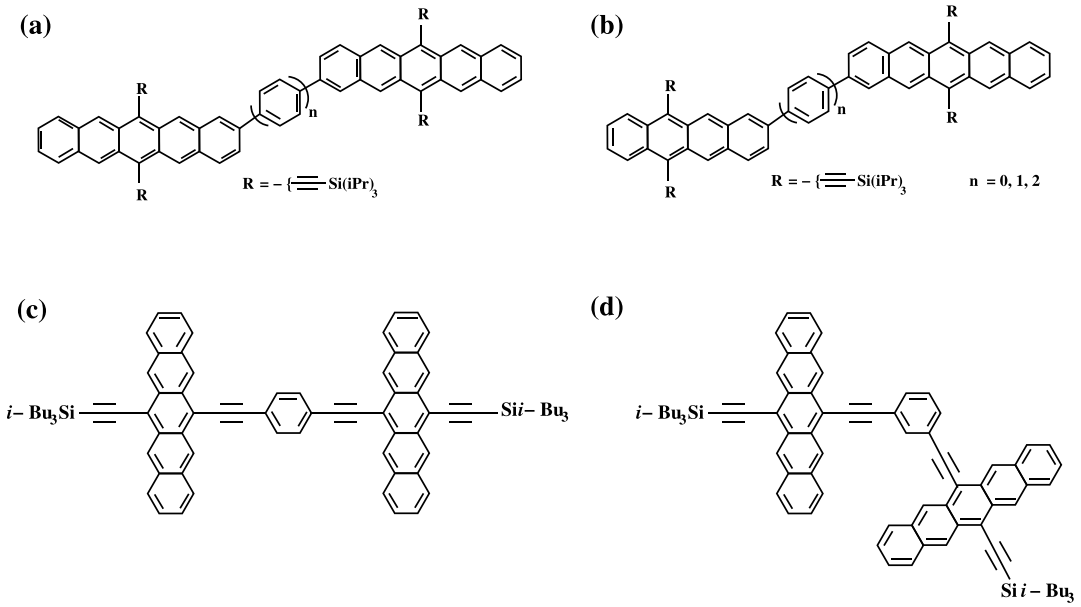

Figure 1. TIPS-acene dimers linked via phenylene spacer groups: (a) bipentacenes BPn, (b) asymmetric pentacene–tetracene dimers PTn, and (c,d) *para*- and *meta*-(bisethynylpentacenyl)benzene dimers, *p*-2 and *m*-2. Computational results on the photophysics of BPn and PTn have been discussed previously.[34,35] Present work focuses on *p*-2 and *m*-2, but comparisons are made with the earlier results on BPn and PTn to point out similarities and differences, as appropriate.

that determine E_b are also of strong interest. Determining these have acquired urgency in recent years with the discovery that the dissociation of $^1(TT)_1$ into two free T_1 takes much longer than what was believed until recently. Instead of hundreds of femtoseconds,[3,25] the completion of SF can take up to nanoseconds.[24,26−32] Thus the dissociation of $^1(TT)_1$, and not the internal conversion of S_0S_1 to $^1(TT)_1$, may be the rate-determining step in SF. Concurrent theoretical work on crystals of pentacene,[33] covalently linked homodimers bipentacenes BPn,[34] and pentacene–tetracene heterodimers PTn[35] has shown that ultrafast excited-state absorptions (ESAs) in the visible range of the electromagnetic spectrum, previously ascribed to T_1, are from the bound $^1(TT)_1$, whose intramonomer excitations overlap in the visible with those of T_1. Many-body calculations for BPn and PTn predicted *additional* $^1(TT)_1$ ESAs in the near infrared (IR) and short-wave IR that are absent in the T_1 spectra. These IR absorptions have subsequently been detected in BPn and PTn[31,32] as well as in oligomers.[18]

BPn and PTn consist of acene monomers linked *longitudinally* through n = 0−3 phenylene linkers (2−2′ links, see Figure 1a,b). The limited geometries investigated theoretically so far raise new questions crucial for understanding the mechanism of ISF. First, are the ESAs in the IR from $^1(TT)_1$ expected in molecular dimers irrespective of topology, or are they unique to specific structural features (such as 2−2′ links)? Second, what is the relationship, if any, between these absorptions and E_b? Finally, since ultrafast measurements in the IR are difficult, can the *qualitative trends* in E_b be guessed from other measurements?

To resolve the above questions, we have investigated theoretically dimers of TIPS-pentacene (TIPS = triisopropylsilyl) that are structurally maximally different from BPn and PTn. Not only are the C−C triple bonds now involved in the intermonomer conjugation (unlike in the 2−2′ linked BP1), the monomers are also linked *transversally* through a phenylene linker (6−6′ link, see Figure 1c,d), as opposed to longitudinally. We investigate theoretically the experimental claim of completed SF in both, which was based on monitoring transient absorptions in the visible alone.[7] We adopt the same short-hand nomenclatures for the molecules as in the original paper,[7] *p*-2 and *m*-2, to label dimers 6−6′ linked through para- and meta-linkages via phenylene. We also examine the theoretical claim[36] that in *m*-2, the spin-quintet $^5(TT)_1$ is lower in energy than the singlet $^1(TT)_1$ and that E_b is negative [which would imply spontaneous direct decay from S_0S_1 to $2 \times (T_1)$]. We report here accurate many-body computational results of ESAs from T_1 and, importantly, $^1(TT)_1$ in *p*-2 and *m*-2 for comparison with experiments. In addition, we report calculations of the spin gap $\Delta_S = E(^5(TT)_1) - E(^1(TT)_1)$ and E_b in *p*-2 and *m*-2 as well as linear polyenes and BP1 to arrive at generic qualitative answers to the questions we have posed above. We recognize that Δ_S and E_b are small, and the uncertainties in our computationally obtained quantities are nonnegligible. We are however confident that the ranges and the overall trend for the quantities computed within our many-body approach are accurate and, more importantly, that the predicted structure–property trends (2−2′ vs 6−6′, and para vs meta links) are correct.

THEORETICAL MODEL, PARAMETRIZATION, AND COMPUTATIONAL METHODS

We consider the π-electron only Pariser–Parr–Pople (PPP) Hamiltonian.[37,38]

$$H = \sum_{\langle ij\rangle,\sigma} t_{ij}(c_{i\sigma}^{\dagger}c_{j\sigma} + c_{j\sigma}^{\dagger}c_{i\sigma}) + U\sum_i n_{i\uparrow}n_{i\downarrow} + \sum_{i<j} V_{ij}(n_i - 1)(n_j - 1) \quad (1)$$

where $c_{i\sigma}^{\dagger}$ creates an electron with spin σ on the p_z orbital of carbon (C) atom i, $n_{i\sigma} = \sum c_{i\sigma}^{\dagger}c_{i\sigma}$ is the number of electrons with spin σ on atom i, and $n_i = \sum_\sigma n_{i\sigma}$ is the total number of

DOI: 10.1021/acs.jpcc.9b09831
J. Phys. Chem. C 2020, 124, 1171−1177

electrons on the atom. We retain electronic hoppings t_{ij} only between the nearest neighbors i and j. U is the Coulomb repulsion between two electrons occupying the p_z orbital of the same C-atom, and V_{ij} is the long-range Coulomb interaction. The average bond lengths within an acene unit are different for the peripheral (1.40 Å) and internal (1.46 Å) C−C bonds.[35] On the basis of a widely used bond length-hopping integral relationship,[39] we have chosen intra-acene peripheral (internal) hopping integrals t_{ij} as −2.4 (−2.2) eV. For the C−C triple bonds, we have chosen t_{ij} = −3.0 eV.[39] It is known that *p*-2 is planar and *m*-2 is nearly planar;[7] we have chosen planar geometries for both and, therefore, interunit C−C hopping integrals −2.2 eV[39] between the TIPS-pentacene monomers and the phenylene linker. We use the screened Ohno parameterization for the long-range Coulomb repulsion, $V_{ij} = U/\kappa\sqrt{1 + 0.6117R_{ij}^{2}}$, where R_{ij} is the distance in Å between C-atoms i and j and κ is an effective dielectric constant.[40] The parameters U and κ were chosen from comparisons to known monomer TIPS-pentacene energies. Monomer $E(S_1)$ is reproduced best with U = 6.7 eV, κ = 1.0. However, the dipole-allowed triplet excitation energy, $E(T_3) - E(T_1)$, of interest here, is best reproduced with U = 7.7 eV, κ = 1.3 [see Table S1, Supporting Information; $E(T_1)$ is almost the same for both parameter sets]. The justification for using U smaller than that within the "standard" Ohno parameters[41] and $\kappa \neq 1$ comes from extensive fittings of wavelength-dependent spectra in π-conjugated polymers[40] as well as polyacenes,[42] with multiple U and κ.

We report results for both sets of close-lying parameters. Our inclusion of both allows obtaining an accurate range for the calculated Δ_S and E_b, whereas the dominant exciton basis wave function components of interest (see below) are the same for the two parameters.

The PPP Hamiltonian allows rigorous many-body calculations of the energies of and ESAs from $^1(TT)_1$ that are not possible for large molecules within first principles approaches. Accurate determination of just the energy of this two electron−two hole (2e−2h) excitation requires including configuration interaction (CI) with at least 4e−4h excitations from the Hartree−Fock (HF) ground state.[43] This continues to be difficult within first principles approaches[4,23] for molecules with more than about 10 π-electrons and certainly for the present case with 58 π-electrons. Calculating ESAs from $^1(TT)_1$, or Δ_S and E_b, make the requirements on the theory even more stringent. We use here a modified version of the multiple reference singles and doubles CI (MRSDCI) approach that was originally developed to include the dominant 1e−1h, 2e−2h, and 4e−4h excitations that best describe any targeted excited state,[22] including $^1(TT)_1$. We have modified the original technique in order to obtain simultaneously the ESA spectrum, by including among the reference configurations not only the minimal basis required to obtain the targeted state but also the configurations that are dipole-coupled to the fundamental reference configurations (see Section B, Supporting Information). Each targeted state (S_1, T_1, $^1(TT)_1$, and $^5(TT)_1$) and the final states of the ESAs from it are thus obtained by solving the same MRSDCI Hamiltonian matrix. In every case, our Hamiltonian matrices have dimensions of several million (see Tables S2 and S3, Supporting Information).

Our calculations are done using a localized exciton basis that allows pictorial representations of eigenstates.[33−35] The Hamiltonian (eq 1) is written as $H = H_{intra} + H_{inter}$, where H_{intra} consists of purely intramolecular terms within eq 1 and H_{inter} consists of the remaining intermolecular terms. HF MOs that are solutions of H_{intra} are obtained in the first step of the calculations. MRSDCI diagonalization of $H_{intra} + H_{inter}$ then yields eigenstates of the complete Hamiltonian as superpositions of many-electron configurations in which these HF MOs are occupied by electrons in all possible manners, including upto 4e−4h excitations. A thorough discussion of the application of the exciton basis that illustrates all finer points can be found in ref 44, which reported exact PPP calculations for *trans*-decapentaene, with H_{intra} describing individual ethylenic units. The advantage of this description is that not only excitations can be classified as predominantly intramonomer versus intermonomer, final states of dipole-allowed optical excitations from any initial state can also be anticipated from the diagrammatic representation of the initial state. The latter constitutes a strong check on the numerical calculations.

Table 1. Calculated Energies of S_1, T_1, $^1(TT)_1$, and $^5(TT)_1$ (in eV) in Polyenes trans-octatetraene (trans-8) and trans-dodecahexaene (trans-12) and Acene Dimers for U = 6.7 eV, κ = 1.0 (Outside Parentheses) and U = 7.7 eV, κ = 1.3 (Inside Parentheses

	$E(S_1)$	$E(T_1)$	$E(^1(TT)_1)$	$E(^5(TT)_1)$
trans-8	3.56 (4.09)	2.06 (1.85)	3.91 (3.69)	6.27 (5.55)
trans-12	2.99 (3.5)	1.75 (1.63)	3.18 (3.03)	4.88 (4.37)
BP1	1.91 (2.09)	1.04 (0.96)	1.95 (1.75)	1.96 (1.76)
p-2	1.81 (1.99)	0.99 (0.91)	1.90 (1.71)	1.95 (1.76)
m-2	1.85 (2.02)	0.972 (0.879)	1.935 (1.736)	1.937 (1.741)

RESULTS AND ANALYSIS

In Table 1 we have given the energies of S_1, T_1, $^1(TT)_1$, and $^5(TT)_1$ for both *p*-2 and *m*-2 for both sets of parameters. We first discuss the singlet, triplet, and $^1(TT)_1$ and then follow up with discussions of $^5(TT)_1$ and our calculated Δ_S and E_b. We have included in the table the same quantities for two linear polyenes as well as for BP1 for comparison and understanding of structure dependence of all quantities. Our calculated $^1(TT)_1$ is either nearly degenerate with or lower in energy than S_1 for both *p*-2 and *m*-2, in agreement with experiments.[7] In Figure 2a we have shown the calculated ground-state absorptions for *p*-2 and *m*-2, whereas Figure 2b,c gives the corresponding wave functions. The weak charge-transfer (CT) absorptions found theoretically are seen at ∼450 nm experimentally (see Figures S14 and S15 of Supporting Information of ref 7). Similar (but stronger) CT absorptions are seen also in BPn and PTn experimentally[6,13] and within our many-body computations.[34,35] There is a subtle difference between the CT contributions to *p*-2 and *m*-2. S_1 in *p*-2 is moderately strongly coupled to the lowest energy CT state (see wave function in Figure 2b). In contrast, the 4% CT contribution to *m*-2 comes almost entirely from the higher energy CT diagrams that also contribute to S_2 in *m*-2 (see wave function in Figure 2c). Because the relative weights of the higher energy configurations in S_2 are very small (see Figure 2c), the absorption to S_2 in *m*-2 is much weaker, which in turn

DOI: 10.1021/acs.jpcc.9b09831
J. Phys. Chem. C 2020, 124, 1171−1177

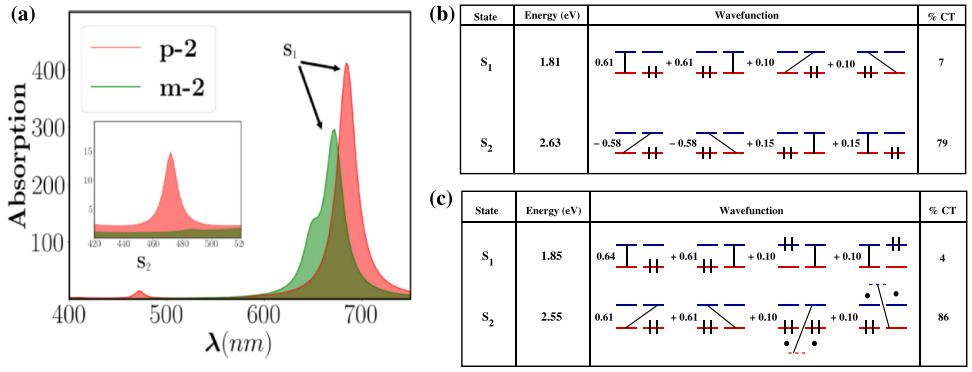

Figure 2. (a) Calculated ground-state absorption spectra for *p*-2 and *m*-2 dimers with U = 6.7 eV and κ = 1.0, to be compared against Figures S15b and S14, respectively, in the Supporting Information of ref 7. The shoulder on the absorption band of *m*-2 is due to absorption to a state that becomes weakly allowed because of the absence of inversion symmetry. The inset shows the relative intensities of the CT absorptions. (b,c) Dominant exciton basis contributions to S_1 and S_2 wave functions in *p*-2 and *m*-2, respectively. The last column gives the percentage CT contribution to the wave function.

is a signature of the weaker coupling between the TIPS monomers in this compound, as is ascertained also from other calculations reported below.

Calculations in the spin-triplet subspace further confirm the difference in the intermonomer couplings between *p*-2 and *m*-2. T_1 in *p*-2 is a superposition of triplet Frenkel excitons in the monomers (see Figure S2a in the Supporting Information), as is true also for BPn and PTn. There exists an excited triplet CT state T_2 that is nearly degenerate with S_2 (see Figure S2a, Supporting Information). The weak coupling between the monomers in *m*-2, suggested already from the singlet wave functions in Figure 2c, leads to extreme localization and triplet states that are unique to *m*-2 among all ISF dimers we have studied so far: instead of aT_1 that is a superposition of Frenkel excitons, triplet eigenstates here occur as distinct degenerate pairs of excitons localized on individual monomers (see Figure S2b in the Supporting Information). In Figure 3a we have shown the calculated ESAs from the T_1 exciton in *p*-2 (red) and *m*-2 (green). The absorptions in the 550−600 nm region, common to both *p*-2 and *m*-2, are due to intramonomer molecular excitations. The absorption at ∼700 nm in *p*-2 is to T_2, which is of CT character and occurs also in BP1 and PT1.[35] Transient absorptions from T_1 are then predicted to be different in *p*-2 and *m*-2.

In Figure 3b, we show schematically why two additional absorptions from $^1(TT)_1$, beyond the intramolecular excitation (i) that overlap with T_1 intramolecular absorptions, are expected for intermediate to strong intermonomer coupling. Determining computationally the higher energy CT absorption (ii) to the final state, referred to as $^1(TT)_2$ hereafter, requires the retention of both a large number of monomer MOs[34] as well as a very large many-electron basis,[22] neither of which are possible outside the PPP approach. Experimentally, the low-energy CT absorption (iii) is more relevant, as this will occur far from the intramolecular absorptions. From the exciton basis wave functions in Figure 2b and the schematic in Figure 3b(iii), we predict S_2 to be the final state of this transient absorption. Assuming $^1(TT)_1$ to be nearly at 2 × $E(T_1)$ or quasidegenerate with S_1, it then becomes possible to estimate the approximate energy of the long wavelength transient absorption of $^1(TT)_1$ from physical arguments alone, viz., it should be close to, though not exactly, $E(S_2) - E(S_1)$.

In Figure 3c, we have given the calculated MRSDCI ESA spectra of $^1(TT)_1$ for both *p*-2 and *m*-2. The CT absorptions to

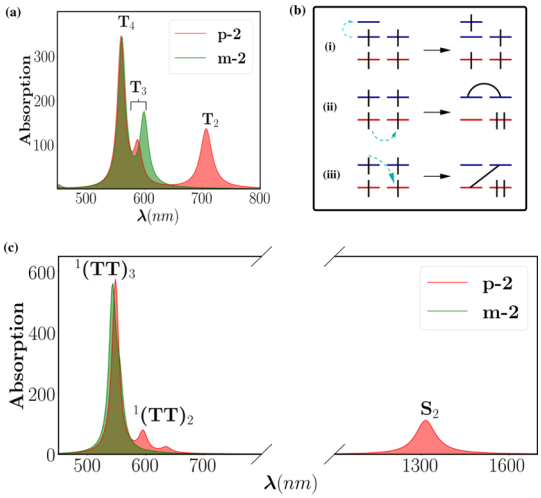

Figure 3. (a) Calculated triplet ESA spectra in *p*-2 (red) and *m*-2 (green), with U = 7.7 eV and κ = 1.3. Absorption near 700 nm in *p*-2 is currently a prediction. Absorption in this region is absent in *m*-2. The initial T_1 and the final states reached in ESA are given in the Supporting Information. (b) Schematics of the expected optical transitions from the bound $^1(TT)_1$. In addition to the monomeric absorption (i) that would overlap with T_1 absorption, two additional CT absorptions (ii) and (iii) are expected. The final state in (iii) is the state S_2 of Figure 2. (c) Calculated ESA spectra of $^1(TT)_1$ in *p*-2 (red) and *m*-2 (green), with U = 7.7 eV and κ = 1.3 eV. The absorption to T_2 in the red to near IR in the free triplet of *p*-2 is absent in the corresponding bound triplet−triplet. Correspondingly, the absorption in the IR at 1300−1400 nm in the bound triplet−triplet of *p*-2 is absent in the free triplet absorption from the same compound.

$^1(TT)_2$ and S_2 for *p*-2 are clearly indicated. As expected from the weak intermonomer coupling in *m*-2, seen already from the calculated ground-state absorption and the triplet ESA, there is negligible CT contribution to $^1(TT)_1$ wave function here (see Figure S3, Supporting Information), leading to vanishing strength of the CT absorption in the IR for *m*-2 in Figure 3c.

We are now in a position to compare the calculated transient absorptions to the experimental ones in ref 7. In what follows, we refer to the experimental figures in the Supporting Information of ref 7, focusing on the false color spectra in Figure S20b,c. The experimental transient absorption in Figure S20b for *m*-2 is very narrow and limited to the visible region, in excellent agreement with the calculated ESA spectra for *m*-2 in

DOI: 10.1021/acs.jpcc.9b09831
J. Phys. Chem. C 2020, 124, 1171−1177

Figure 3a as well as Figure 3c. In contrast, additional absorption extending into the IR (1.2−1.4 eV) is clearly seen in the false color spectrum in Figure S20c for *p*-2, also in excellent agreement with our calculated $^1(TT)_1$ spectrum for *p*-2 in Figure 3c (weak quantitative deviations between the calculated and experimental ESA energies are to be expected within the difficult many-body calculations). Furthermore, the considerably broader experimental transient absorption in *p*-2 in the visible (see false color spectrum in Figure S20c in ref 7) is in agreement with the calculated ESA spectrum for *p*-2 Figure 3c, where contribution from absorption to the high-energy CT state $^1(TT)_2$ occurs. We also draw attention to the 1.8 eV (700 nm) region where T_1 should absorb, but the experimental photoinduced absorption is very weak. On the basis of the persistence of the transient absorption in the IR through the duration of the experiment,[7] we conclude that the lifetime of the bound $^1(TT)_1$ in *p*-2 is far longer than what had been assumed before, and dissociation to free triplets does not occur here.

In Table 2 we have given our computed Δ_S and E_b for all compounds in Table 1, also for both sets of parameters. There

Table 2. Calculated Spin Gap Δ_S and Binding Energy E_b of $^1(TT)_1$ in Polyenes and Acene Dimers for U = 6.7 eV, κ = 1.0 (Outside Parentheses) and U = 7.7 eV, κ = 1.3 (Inside Parentheses)

	Δ_S	E_b
trans-8	1.86 (2.36)	0.21 (0.01)
trans-12	1.34 (1.70)	0.32 (0.23)
BP1	0.01 (0.02)	0.13 (0.17)
p-2	0.05 (0.05)	0.08 (0.11)
m-2	0.005 (0.002)	0.009 (0.021)

is no correlation between Δ_S and E_b in the polyenes, which are included for comparison only. The very large Δ_S and its decrease with increasing length are both anticipated from the different dominant MO occupancies (see Figure S4 in the Supporting Information) in $^5(TT)_1$ versus $^1(TT)_1$. In contrast to Δ_S, which decreases with length, the calculated E_b increases with length in this regime, which is counterintuitive. This is a finite-size effect. The increase here is because in the shortest polyenes, the two individual triplets in $^1(TT)_1$ are strongly overlapping (see schematics in Figure S5 of the Supporting Information). Whereas T_1 can have optimal length (or close to it) even in short polyenes, the triplets in $^1(TT)_1$ overlap and the $^1(TT)_1$ is artificially confined, the combined effect of which is to increase the energy of the biexciton relative to the free triplets[45] and to lower E_b. Hence, E_b here increases with polyene length until the polyene reaches an optimal length where the triplet overlap is optimal and is decided by the spin−spin coupling alone, beyond which E_b should decrease monotonically. The situation is different in the acene dimers, where the triplets in $^1(TT)_1$ and $^5(TT)_1$ occupy different monomers (see Figure S3, Supporting Information) and are hence nonoverlapping. The orbital occupancies in the exciton basis are thus the same for the spin-singlet and spin-quintet triplet−triplet. Δ_S and E_b now depend only on intermonomer coupling, and there is one-to-one correspondence between them. They are, however, not equal, as is sometimes assumed.[46] This is because between two free triplets, there can be no CT by definition, whereas in $^5(TT)_1$ of any coupled species in which the individual units are larger than two level system, there is always some CT involving nondegenerate MOs, as is indicated in Figure 4. E_b is, therefore, slightly larger

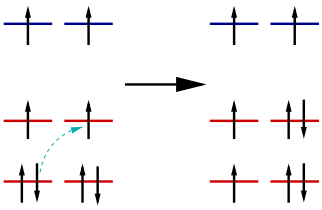

Figure 4. Schematic of the CT that will occur in the bound $^5(TT)_1$ to lower its energy relative to a pair of free, uncorrelated triplets.

than Δ_S, as found in Table 2. We see that our calculated quantities in BP1 and *p*-2 are close to one another. Whereas structural relaxation effects have been ignored in our calculations, we note that in both T_1 and $^1(TT)_1$, the triplet wave functions occupy individual monomers and the contributions of structural relaxations to Δ_S and E_b will likely cancel, at least partially, in the respective energy differences. E_b in both BP1 and *p*-2 likely exceeds thermal energy, explaining the long lifetime of $^1(TT)_1$.

Assumption of frozen spin configurations on the alternant (bipartite) phenylene linker suggests ferromagnetic spin−spin correlation between substituents at meta positions and negative Δ_S and E_b in *m*-2.[36] From our many-body calculations, we find both to be positive, albeit very small. This weak deviation from the prediction in ref 36 can be explained within the valence bond (VB) theory, as indicated in Figure 5. The meta-linkage can be described by the spin-singlet

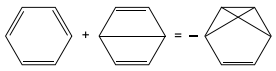

Figure 5. Linear relationship between VB diagram with crossed bonds and Kekulé and Dewar VB diagrams in benzene.

VB diagram with "crossing" bonds, which is a superposition of the more familiar Kekulé and Dewar VB diagrams. Weak but nonzero CT will occur across the spin-singlet bond between the monomers even with meta-linkage, lowering the energy of $^1(TT)_1$ relative to $^5(TT)_1$ very slightly and also making E_b positive. Inclusion of realistic second-neighbor electron hopping in eq 1 will further enhance Δ_S and E_b.

CONCLUSIONS

To conclude, for moderate to strong intermonomer coupling in ISF compounds, transient absorption measurements in the IR are essential for distinguishing between free triplets and the bound triplet−triplet in ISF compounds. In such cases, both the free triplet and the triplet−triplet ESAs in the covalently linked dimers are different from the triplet absorption in the monomer while also being different from one another (see Figure 3a,c). This conclusion is independent of the detailed geometry and is valid for both longitudinal (2−2′) and transverse (6−6′) coupling between acene monomers. Comparison with experimental ultrafast spectroscopy in *p*-2 leads to the conclusion that $^1(TT)_1$ here has a very long lifetime. Since a long lifetime opens up various channels of $^1(TT)_1$ decay, our calculations provide a diagnostic tool to experimentalists to preselect ISF compounds for application to solar cells.

DOI: 10.1021/acs.jpcc.9b09831
J. Phys. Chem. C 2020, 124, 1171−1177

In contrast to *p*-2, we find that the intermonomer coupling in *m*-2 is extremely weak, to the extent that the triplet wave functions here occur as degenerate pairs, with the lowest two consisting of the Frenkel excitons localized on one or the other TIPS-pentacene monomer. Thus, topology can indeed play a very strong role in ISF. We agree with the authors of ref 36 that Δ_S and E_b are tiny, except that we find these to be still weakly positive. Going beyond the frozen spin configuration and proper consideration of electron correlation effects is essential to arrive at the correct state ordering within the triplet−triplet manifold. Spontaneous generation of $^5(TT)_1$ as well as of free triplets in *m*-2, due to thermal effects or structural relaxations not taken into consideration in our calculations, are both possible. We believe that similar tiny energy differences also characterize BP3, where $^5(TT)_1$ has been detected and characterized.[29] Neither the experimental nor the computational free triplet and triplet−triplet ESA spectra are distinguishable in *m*-2. It is therefore conceivable, even likely that free triplets are indeed generated in *m*-2, as claimed in ref 7. In agreement with our conclusion, it has been found that in meta-linked BP1, photoexcitation leads to significant free triplet population lasting into microseconds, in contrast to the "usual" para-linked BP1, where there is little free triplet generation (private communication, M. Sfeir). Our conclusions regarding free triplet generation are slightly different from those in ref 17, which investigated tetracene dimers and concluded that free triplets are generated from the para but not the meta isomer. It is conceivable that the difference, particularly in the case of the meta compound, arises from $^1(TT)_1$ in the tetracene dimer occurring above S_1 (this would explain the fast radiative relaxation here). Ultrafast spectroscopy here was carried out only in the visible wavelength range. Extending these measurements to the IR should provide additional valuable information.

Two other observations are worthy of noting. First, our calculations indicate that not only $^1(TT)_1$ ESA but even the ground-state absorption and the free triplet ESA provide information on the strength of the intermonomer coupling. Second, the same intermonomer electronic coupling that presumably drives a fast S_1 to $^1(TT)_1$ internal conversion slows down the $^1(TT)_1$ dissociation. For efficient application of SF, this conundrum has to be resolved.

■ ASSOCIATED CONTENT

Supporting Information

The Supporting Information is available free of charge at https://pubs.acs.org/doi/10.1021/acs.jpcc.9b09831.

Results of calculations of energies of S_1, T_1, and the lowest ESA from T_1 in the TIPS monomer, MRSDCI approach for simultaneously calculating the energy of target excited state and ESA from it, Hamiltonian matrix dimensions for the singlet and triplet subspaces in the TIPS-pentacene monomer, *p*-2 and *m*-2, lowest triplets and excited states reached by ESA in *p*-2 and *m*-2, lowest triplet−triplet and excited states reached by ESA in *p*-2 and *m*-2, MO occupancies of $^1(TT)_1$ and and $^5(TT)_1$ in linear polyenes, and relative overlaps between triplets in $^1(TT)_1$ in short versus long polyenes (PDF)

■ AUTHOR INFORMATION

Corresponding Author

*E-mail: mazumdar@email.arizona.edu.

ORCID

Sumit Mazumdar: 0000-0002-1010-4044

Notes

The authors declare no competing financial interest.

■ ACKNOWLEDGMENTS

The authors are grateful to Professor Alok Shukla (IIT Bombay) for significant help with the computations and to Professor Matthew Sfeir (The Graduate Center, CUNY) for discussions of unpublished results on meta-BP1. The authors acknowledge support from NSF-CHE-1764152.

■ REFERENCES

(1) Johnson, J. C.; Nozik, A. J.; Michl, J. The Role of Chromophore Coupling in Singlet Fission. *Acc. Chem. Res.* **2013**, *46*, 1290−1299.

(2) Smith, M. B.; Michl, J. Recent Advances in Singlet Fission. *Annu. Rev. Phys. Chem.* **2013**, *64*, 361−386.

(3) Rao, A.; Friend, R. H. Harnessing singlet exciton fission to break the Shockley-Queisser limit. *Nat. Rev.* **2017**, *2*, 17063.

(4) Casanova, D. Theoretical Modeling of Singlet Fission. *Chem. Rev.* **2018**, *118*, 7164−7207.

(5) Shockley, W.; Queisser, H. J. Detailed Balance Limit of Efficiency of p-n Junction Solar Cells. *J. Appl. Phys.* **1961**, *32*, 510−519.

(6) Sanders, S. N.; Kumarasamy, E.; Pun, A. B.; Trinh, M. T.; Choi, B.; Xia, J.; Taffet, E. J.; Low, J. Z.; Miller, J. R.; Roy, X.; et al. Quantitative Intramolecular Singlet Fission in Bipentacenes. *J. Am. Chem. Soc.* **2015**, *137*, 8965−8972.

(7) Zirzlmeier, J.; Lehnherr, D.; Coto, P. B.; Chernick, E. T.; Casillas, R.; Basel, B. S.; Thoss, M.; Tykwinski, R. R.; Guldi, D. M. Singlet fission in pentacene dimers. *Proc. Natl. Acad. Sci. U.S.A.* **2015**, *112*, 5325−5330.

(8) Lukman, S.; Musser, A. J.; Chen, K.; Athanasopoulos, S.; Yong, C. K.; Zeng, Z.; Ye, Q.; Chi, C.; Hodgkiss, J. M.; Wu, J.; Friend, R. H.; Greenham, N. C. Tuneable Singlet Exciton Fission and Triplet-Triplet Annihilation in an Orthogonal Pentacene Dimer. *Adv. Funct. Mater.* **2015**, *25*, 5452−5461.

(9) Busby, E.; Xia, J.; Wu, Q.; Low, J. Z.; Song, R.; Miller, J. R.; Zhu, X.-Y.; Campos, L. M.; Sfeir, M. Y. A design strategy for intramolecular singlet fission mediated by charge-transfer states in donor-acceptor organic materials. *Nat. Mater.* **2015**, *14*, 426−433.

(10) Fuemmeler, E. G.; Sanders, S. N.; Pun, A. B.; Kumarasamy, E.; Zeng, T.; Miyata, K.; Steigerwald, M. L.; Zhu, X.-Y.; Sfeir, M. Y.; Campos, L. M.; et al. A Direct mechanism of Ultrafast Intramolecular Singlet Fission in Pentacene Dimers. *ACS Cent. Sci.* **2016**, *2*, 316−324.

(11) Sakuma, T.; Sakai, H.; Araki, Y.; Mori, T.; Wada, T.; Tkachenko, N. V.; Hasobe, T. Long-Lived Triplet Excited States of Bent-Shaped Pentacene Dimers by Intramolecular Singlet Fission. *J. Phys. Chem. A* **2016**, *120*, 1867−1875.

(12) Sanders, S. N.; Kumarasamy, E.; Pun, A. B.; Steigerwald, M. L.; Sfeir, M. Y.; Campos, L. M. Intramolecular Singlet Fission in Oligoacene Heterodimers. *Angew. Chem., Int. Ed.* **2016**, *55*, 3373−3377.

(13) Sanders, S. N.; Kumarasamy, E.; Pun, A. B.; Appavoo, K.; Steigerwald, M. L.; Campos, L. M.; Sfeir, M. Y. Exciton Correlations in Intramolecular Singlet Fission. *J. Am. Chem. Soc.* **2016**, *138*, 7289−7297.

(14) Korovina, N. V.; Das, S.; Nett, Z.; Feng, X.; Joy, J.; Haiges, R.; Krylov, A. I.; Bradforth, S. E.; Thompson, M. E. Singlet Fission in a Covalently Linked Cofacial Alkynyltetracene Dimer. *J. Am. Chem. Soc.* **2016**, *138*, 617−627.

(15) Liu, H.; Nichols, V. M.; Shen, L.; Jahansouz, S.; Chen, Y.; Hanson, K. M.; Bardeen, C. J.; Li, X. Synthesis and photophysical properties of a face-to-face stacked tetracene dimer. *Phys. Chem. Chem. Phys.* **2015**, *17*, 6523−6531.

DOI: 10.1021/acs.jpcc.9b09831
J. Phys. Chem. C 2020, 124, 1171−1177

(16) Margulies, E. A.; Miller, C. E.; Wu, Y.; Ma, L.; Schatz, G. C.; Young, R. M.; Wasielewski, M. R. Enabling singlet fission by controlling intramolecular π stacked covalent terrylenediimide dimers. *Nat. Chem.* **2016**, *8*, 1120−1125.
(17) Korovina, N. V.; Joy, J.; Feng, X.; Feltenberger, C.; Krylov, A. I.; Bradforth, S. E.; Thompson, M. E. Linker-Dependent Singlet Fission in Tetracene Dimers. *J. Am. Chem. Soc.* **2018**, *140*, 10179−10190.
(18) Pun, A. B.; Asadpoordarvish, A.; Kumarasamy, E.; Tayebjee, M. J. Y.; Niesner, D.; McCamey, D. R.; Sanders, S. N.; Campos, L. M.; Sfeir, M. Y. Ultra-fast intramolecular singlet fission to persistent multiexcitons by molecular design. *Nat. Chem.* **2019**, *11*, 821−828.
(19) Hudson, B. S.; Kohler, B. E.; Schulten, K. Linear Polyene Electronic−Structure and Potential Surfaces. *Excited States* **1982**, *6*, 1−95.
(20) Ramasesha, S.; Soos, Z. G. Diagrammatic valence-bond theory for finite-model Hamiltonians. *Int. J. Quantum Chem.* **1984**, *25*, 1003−1021.
(21) Ramasesha, S.; Soos, Z. G. Correlated States in Linear Polyene, Radicals, And Ions - Exact PPP Transition Moments and Spin Densities. *J. Chem. Phys.* **1984**, *80*, 3278−3287.
(22) Tavan, P.; Schulten, K. Electronic Excitations in Finite and Infinite Polyenes. *Phys. Rev. B: Condens. Matter Mater. Phys.* **1987**, *36*, 4337−4358.
(23) Kim, H.; Zimmerman, P. M. Coupled double triplet state in singlet fission. *Phys. Chem. Chem. Phys.* **2018**, *20*, 30083−30094.
(24) Musser, A. J.; Clark, J. Triplet-Pair States in Organic Semiconductors. *Annu. Rev. Phys. Chem.* **2019**, *70*, 323−351.
(25) Wilson, M. W. B.; Rao, A.; Johnson, K.; Gélinas, S.; di Pietro, R.; Clark, J.; Friend, R. H. Temperature-Independent Singlet Exciton Fission in Tetracene. *J. Am. Chem. Soc.* **2013**, *135*, 16680−16688.
(26) Yong, C. K.; Musser, A. J.; Bayliss, S. L.; Lukman, S.; Tamura, H.; Bubnova, O.; Hallani, R. K.; Meneau, A.; Resel, R.; Maruyama, M.; et al. The entangled triplet pair state in acene and heteroacene materials. *Nat. Commun.* **2017**, *8*, 15953.
(27) Stern, H. L.; Cheminal, A.; Yost, S. R.; Broch, K.; Bayliss, S. L.; Chen, K.; Tabachnyk, M.; Thorley, K.; Greenham, N.; Hodgkiss, J. M.; et al. Vibronically coherent ultrafast triplet-pair formation and subsequent thermally activated dissociation control efficient endothermic singlet fission. *Nat. Chem.* **2017**, *9*, 1205−1212.
(28) Weiss, L. R.; Bayliss, S. L.; Kraffert, F.; Thorley, K. J.; Anthony, J. E.; Bittl, R.; Friend, R. H.; Rao, A.; Greenham, N. C.; Behrends, J. Strongly exchange-coupled triplet pairs in an organic semiconductor. *Nat. Phys.* **2017**, *13*, 176−181.
(29) Tayebjee, M. J. Y.; Sanders, S. N.; Kumarasamy, E.; Campos, L. M.; Sfeir, M. Y.; McCamey, D. R. Quintet multiexciton dynamics in singlet fission. *Nat. Phys.* **2017**, *13*, 182−188.
(30) Basel, B. S.; Zirzlmeier, J.; Hetzer, C.; Phelan, B. T.; Krzyaniak, M. D.; Reddy, S. R.; Coto, P. B.; Horwitz, N. E.; Young, R. M.; White, F. J.; et al. Unified model for singlet fission within a non-conjugated covalent pentacene dimer. *Nat. Commun.* **2017**, *8*, 15171.
(31) Trinh, M. T.; Pinkard, A.; Pun, A. B.; Sanders, S. N.; Kumarasamy, E.; Sfeir, M. Y.; Campos, L. M.; Roy, X.; Zhu, X.-Y. Distinct properties of the triplet pair state from singlet fission. *Sci. Adv.* **2017**, *3*, No. e1700241.
(32) Miyata, K.; Conrad-Burton, F. S.; Geyer, F. L.; Zhu, X.-Y. Triplet Pair States in Singlet Fission. *Chem. Rev.* **2019**, *119*, 4261−4292.
(33) Khan, S.; Mazumdar, S. Theory of Transient Excited State Absorptions in Pentacene and Derivatives: Triplet-Triplet Biexciton versus Free Triplets. *J. Phys. Chem. Lett.* **2017**, *8*, 5943−5948.
(34) Khan, S.; Mazumdar, S. Diagrammatic Exciton Basis Theory of the Photophysics of Pentacene Dimers. *J. Phys. Chem. Lett.* **2017**, *8*, 4468−4478.
(35) Khan, S.; Mazumdar, S. Optical probes of the quantum-entangled triplet-triplet state in a heteroacene dimer. *Phys. Rev. B* **2018**, *98*, 165202.
(36) Abraham, V.; Mayhall, N. J. Simple Rule To Predict Boundedness of Multiexciton States in Covalently Linked Singlet-Fission Dimers. *J. Phys. Chem. Lett.* **2017**, *8*, 5472−5478.
(37) Pariser, R.; Parr, R. G. A Semi-Empirical theory of the electronic spectra and electronic structure of complex unsaturated molecules II. *J. Chem. Phys.* **1953**, *21*, 767−776.
(38) Pople, J. A. Electron interaction in unsaturated hydrocarbons. *Trans. Faraday Soc.* **1953**, *49*, 1375−1385.
(39) Ducasse, I. R.; Miller, T. E.; Soos, Z. G. Correlated states in finite polyenes: Exact PPP results. *J. Chem. Phys.* **1982**, *76*, 4094−4104.
(40) Chandross, M.; Mazumdar, S. Coulomb interactions and linear, nonlinear, and triplet absorption in poly(para-phenylenevinylene). *Phys. Rev. B: Condens. Matter Mater. Phys.* **1997**, *55*, 1497−1504.
(41) Ohno, K. Some remarks on the Pariser-Parr-Pople method. *Theor. Chim. Acta* **1964**, *2*, 219−227.
(42) Sony, P.; Shukla, A. Large-scale correlated calculations of linear optical absorption and low-lying excited states of polyacenes: Pariser-Parr-Pople Hamiltonian. *Phys. Rev. B: Condens. Matter Mater. Phys.* **2007**, *75*, 155208.
(43) Tavan, P.; Schulten, K. The 2^1A_g-1^1B_u energy gap in the polyenes: An extended configuration interaction study. *J. Chem. Phys.* **1979**, *70*, 5407−5413.
(44) Chandross, M.; Shimoi, Y.; Mazumdar, S. Diagrammatic exciton-basis valence-bond theory of linear polyenes. *Phys. Rev. B: Condens. Matter Mater. Phys.* **1999**, *59*, 4822−4838.
(45) Guo, F.; Chandross, M.; Mazumdar, S. Stable Biexcitons in Conjugated Polymers. *Phys. Rev. Lett.* **1995**, *74*, 2086−2089.
(46) Feng, X.; Krylov, A. I. On couplings and excimers: lessons from studies of singlet fission in covalently linked tetracene dimers. *Phys. Chem. Chem. Phys.* **2016**, *18*, 7751−7761.

DOI: 10.1021/acs.jpcc.9b09831
J. Phys. Chem. C 2020, 124, 1171−1177